Available online at www.sciencedirect.com
ScienceDirect
Journal of Power Sources 179 (2008) 700–710
JOURNAL OF POWER SOURCES
www.elsevier.com/locate/jpowsour

A theoretical model of the membrane electrode assembly of liquid feed direct methanol fuel cell with consideration of water and methanol crossover

Ken-Ming Yin *

Department of Chemical Engineering and Materials Science, Yuan-Ze University, 135 Yuan-Tung Road, Chung-Li, Taoyuan 32003, Taiwan, ROC

Received 5 December 2007; received in revised form 3 January 2008; accepted 4 January 2008
Available online 12 January 2008

Abstract

An algebraic model of the membrane electrode assembly of the direct methanol fuel cell is developed, which considers the simultaneous liquid water and methanol crossover effects, and the associated electrochemical reactions. The respective anodic and cathodic polarization curves can be predicted using this model. Methanol concentration profile and flux are correlated explicitly with the operating conditions and water transport rate. The cathode mixed potential effect induced by the methanol crossover is included and the subsequent cell voltage loss is identified. Water crossover is influenced by the capillary pressure equilibrium and hydrophobic property within the cathode gas diffusion layer. The model can be used to evaluate the cell performance at various working parameters such as membrane thickness, methanol feed concentration, and hydrophobicity of the cathode gas diffuser.

Keywords: Direct methanol fuel cell; Membrane electrode assembly; Water transport; Methanol crossover; Mixed potential

1. Introduction

One critical issue of the research on direct methanol fuel cell (DMFC) is to reduce methanol crossover through the polymer electrolyte membrane [1–4]. The permeation of methanol not only reduces the fuel efficiency but also causes a voltage decline in the cathode due to the internal short-circuit formed by the parasitic reactions of methanol oxidation and the oxygen reduction [5–13]. Another requirement, especially for a portable DMFC, is the retardation of water transport through the polymer membrane. Due to the electro-osmotic drag of water across the membrane, the use of concentrated methanol solution in the anode compartment is not feasible [14–18]. Since water is one of the reactants for methanol oxidation, the anodic limiting species may be switched from methanol to water once water loss is severe in the anode compartment. Condenser is needed to collect water in the cathode and to recycle it to the anode; thus, the design of the portable DMFC becomes much complicated and costly. The cathode gas diffusion layer is normally hydrophobic treated to induce a capillary pressure to lessen water permeation from the anode. An extension of this concept is to fabricate an extra thin micro-porous layer between the catalyst layer and the cathode gas diffusion layer [16–20]. With the incorporation of a high hydrophobic and low porosity carbon layer, the induced capillary pressure is further extended, while the impetus to the oxygen diffusion is not serious due to the thinness of the micro-layer.

The modeling works on the DMFC with attention on the methanol crossover can be found in [5–13]. Scott and co-workers [6,7] treated the cathode voltage loss due to methanol crossover as a fixed value. Kulikovsky [8,9] considered the effect of channel flow on the cathode mixed potential, and found that a narrow zone of local current bridge which short-circuits the cell at a small current load. The inclusion of water transport phenomenon, in addition to the methanol crossover, was developed only recently [21–28]. It is noted that most water transport included models are based on the computational fluid dynamics except a few analytical works in Refs. [21,22]. Sandhu et al.

* Tel.: +886 3 4638800x2556; fax: +886 3 4559373.
E-mail address: cekenyin@saturn.yzu.edu.tw.

0378-7753/$ – see front matter © 2008 Elsevier B.V. All rights reserved.
doi:10.1016/j.jpowsour.2008.01.008

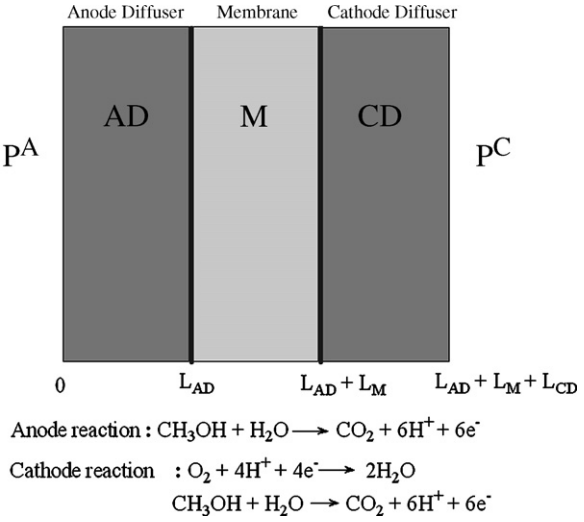

Fig. 1. Schematic of the membrane electrode assembly of DMFC.

[21] algebraically formulated the methanol and water crossover equations but only limited to the membrane region without consideration of the respective anode and cathode electrochemical reactions. The analytical derivation by Shi et al. [22] was also on the membrane region that focused on the water flow and membrane dehydration; methanol crossover and electrochemical kinetics were not included.

The purpose of present work is to develop an efficient algebraic model to elucidate the simultaneous water and methanol crossover phenomena as well as their influence on the cell performance. To limit the scope of this study, only membrane electrode assembly (MEA) is considered, while the flow channel effect is not included. The interplay of mass transport and associated electrochemical reactions is stressed. Algebraic while mechanistic-based model gives an explicit relationship between the important operating parameters and the physical characteristics of the MEA.

2. Mathematical model

Schematic of the studied region is depicted in Fig. 1. The assumptions made in this one-dimensional algebraic model are listed:

(1) The anode and cathode catalyst layers are treated as planes of no thickness. That is, possible concentration variations within the catalyst layers are not considered.
(2) The membrane is fully hydrated.
(3) Electrochemical kinetics of methanol oxidation and oxygen reduction is described by the Tafel equation.
(4) Because the over-potential for the methanol oxidation at cathode is high, it is assumed that the permeated methanol is consumed instantaneously at the membrane/cathode diffuser interface [11,13].
(5) The effect of CO_2 gas bubbles generated in the anode catalyst layer is neglected.

2.1. Liquid water flow

Water conservation within the anode diffuser (AD):

$$\frac{\mathrm{d}N_{\mathrm{H_2O}}^{\mathrm{AD}}}{\mathrm{d}x} = 0 \tag{1}$$

where water flux is governed by the Darcy's law:

$$N_{\mathrm{H_2O}}^{\mathrm{AD}} = -\frac{k_{\mathrm{p}}^{\mathrm{AD}}}{\nu}\frac{\mathrm{d}P_{\mathrm{l}}}{\mathrm{d}x} \tag{2}$$

$k_{\mathrm{p}}^{\mathrm{AD}}$ is the liquid permeability in the anode diffuser, ν ($=\mu/\rho$) the liquid kinematic viscosity defined as the ratio of liquid viscosity and molar density, P_{l} is the local liquid pressure.

Water conservation within the membrane (M):

$$\frac{\mathrm{d}N_{\mathrm{H_2O}}^{\mathrm{M}}}{\mathrm{d}x} = 0 \tag{3}$$

The water flux in membrane phase is driven by the pressure gradient and the electro-osmotic drag:

$$N_{\mathrm{H_2O}}^{\mathrm{M}} = -\frac{k_{\mathrm{p}}^{\mathrm{M}}}{\nu}\frac{\mathrm{d}P_{\mathrm{l}}}{\mathrm{d}x} + \frac{n_{\mathrm{d}}^{\mathrm{H_2O}} I}{F} \tag{4}$$

Water conservation within the cathode diffuser (CD):

$$\frac{\mathrm{d}N_{\mathrm{H_2O}}^{\mathrm{CD}}}{\mathrm{d}x} = 0 \tag{5}$$

Water flux is caused by hydraulic pressure gradient:

$$N_{\mathrm{H_2O}}^{\mathrm{CD}} = -\frac{k_{\mathrm{p}}^{\mathrm{CD}} k_{\mathrm{rl}}^{\mathrm{CD}}}{\nu}\frac{\mathrm{d}P_{\mathrm{l}}}{\mathrm{d}x} \tag{6}$$

$k_{\mathrm{p}}^{\mathrm{CD}}$ is the permeability of water in the carbon fiber matrix. Within the porous structure of the cathode diffusion layer, oxygen gas diffuses in the non-flooding fraction of the void space. The permeability of water transfer is modified by the relative permeability, $k_{\mathrm{rl}}^{\mathrm{CD}}$, expressed as a function of water saturation $k_{\mathrm{rl}}^{\mathrm{CD}} = s^3$ [29]. Water saturation s is determined by the capillary equilibrium between the gas and liquid phases, given as follows [29]:

$$P_{\mathrm{c}} = P^{\mathrm{C}} - P_{\mathrm{l}} = \sigma\cos\theta_{\mathrm{c}}\left(\frac{\varepsilon_{\mathrm{CD}}}{k_{\mathrm{p}}^{\mathrm{CD}}}\right)^{0.5} J(s) \tag{7}$$

P_{c} is the capillary pressure, P^{C} the cathode gas pressure, $\varepsilon_{\mathrm{CD}}$ the porosity within cathode porous medium, θ_{c} the contact angel, σ the surface tension, and $J(s)$ is the Leverette function of the water saturation [30]:

$$J(s) = 1.417s - 2.12s^2 + 1.263s^3 \quad \text{for hydrophobic medium, } \theta_{\mathrm{c}} > 90^\circ \tag{8a}$$

$$J(s) = 1.417(1-s) - 2.12(1-s)^2 + 1.263(1-s)^3 \quad \text{for hydrophilic medium } \theta_{\mathrm{c}} < 90^\circ \tag{8b}$$

Water balances on the anode reaction plane (AD/M interface) and the cathode reaction plane (M/CD interface) are given,

respectively:

$$N_{H_2O}^{M} = N_{H_2O}^{AD} - \frac{I}{6F} \tag{9}$$

$$N_{H_2O}^{CD} = N_{H_2O}^{M} + \frac{I_o}{2F} - \frac{I_{leak}}{6F} \tag{10}$$

I is the cell current density, I_o the partial current density of oxygen reduction, and I_{leak} is the leaking current density caused by the oxidation of permeated methanol on the cathode catalyst.

An overall current conservation can be expressed in Eq. (11), which states that the oxygen consumption is balanced by the oxidation of methanol in the anode plus that occurred in the cathode:

$$I_o = I + I_{leak} \tag{11}$$

Integration of Eq. (2), one obtains:

$$P^{AD/M} = P^{A} - \frac{\nu N_{H_2O}^{AD} L_{AD}}{k_p^{AD}} \tag{12}$$

Integrating of Eq. (4) with the aid of Eqs. (9) and (12):

$$P^{M/CD} = P^{A} + \frac{\nu L_M I}{k_p^M F}\left(\frac{1}{6} + n_d^{H_2O}\right) - \nu N_{H_2O}^{AD}\left(\frac{L_M}{k_p^M} + \frac{L_{AD}}{k_p^{AD}}\right) \tag{13}$$

In combination of Eqs. (7) and (13), one has:

$$P^{C} - P^{A} = \frac{\nu L_M I}{k_p^M F}\left(\frac{1}{6} + n_d^{H_2O}\right) - \nu N_{H_2O}^{AD}\left(\frac{L_M}{k_p^M} + \frac{L_{AD}}{k_p^{AD}}\right) + \sigma \cos\theta_c \left(\frac{\varepsilon_{CD}}{k_p^{CD}}\right)^{0.5} J(s_{M/CD}) \tag{14}$$

where $s_{M/CD}$ is the water saturation at the M/CD interface.

With the aid of Eqs. (7)–(11), Eq. (6) can be integrated over the cathode diffusion layer by letting water saturation zero at the interface of the gas diffuser and flow channel:

$$\left(N_{H_2O}^{AD} + \frac{I_o}{3F}\right) = \frac{\rho \cos\theta_C (\varepsilon_{CD} k_p^{CD})^{0.5}}{\nu L_{CD}} (-0.35425 s_{M/CD}^4 + 0.848 s_{M/CD}^5 - 0.6315 s_{M/CD}^6) \quad \text{for } \theta_c > 90^\circ \tag{15a}$$

and

$$\left(N_{H_2O}^{AD} + \frac{I_o}{3F}\right) = \frac{\rho \cos\theta_C (\varepsilon_{CD} k_p^{CD})^{0.5}}{\nu L_{CD}} (0.2415 s_{M/CD}^4 - 0.6676 s_{M/CD}^5 + 0.6315 s_{M/CD}^6) \quad \text{for } \theta_c < 90^\circ \tag{15b}$$

2.2. Methanol transport

Mass conservation of methanol within the anode diffuser (AD):

$$\frac{dN_m^{AD}}{dx} = 0 \tag{16}$$

Methanol flux is contributed by diffusion and convection:

$$N_m^{AD} = -D_m^{AD}\frac{dC_m}{dx} + \zeta'' C_m (N_{H_2O}^{AD} + N_m^{AD}) \tag{17}$$

D_m^{AD} is the void fraction corrected diffusivity using Bruggerman's correlation [31]. For the dilute solution, mole fraction of methanol can be approximated by $\zeta'' C_m$, where ζ'' is the molecular weight of water.

Eq. (17) can be integrated with the boundary condition $C_m = C_m^b$ at $x = 0$:

$$C_m = \frac{N_m^{AD}}{\zeta''(N_{H_2O}^{AD} + N_m^{AD})}\left\{1 - \exp\left[\frac{\zeta''(N_{H_2O}^{AD} + N_m^{AD})x}{D_m^{AD}}\right]\right\} + C_m^b \exp\left[\frac{\zeta''(N_{H_2O}^{AD} + N_m^{AD})x}{D_m^{AD}}\right] \tag{18}$$

C_m at AD/M interface is simply:

$$C_m^{AD/M} = \frac{N_m^{AD}}{\zeta''(N_{H_2O}^{AD} + N_m^{AD})}\left\{1 - \exp\left[\frac{\zeta''(N_{H_2O}^{AD} + N_m^{AD})L_{AD}}{D_m^{AD}}\right]\right\} + C_m^b \exp\left[\frac{\zeta''(N_{H_2O}^{AD} + N_m^{AD})L_{AD}}{D_m^{AD}}\right] \tag{19}$$

Mass conservation of methanol within the membrane phase (M) is

$$\frac{dN_m^{M}}{dx} = 0 \tag{20}$$

Methanol flux is expressed as follows:

$$N_m^{M} = -D_m^{M}\frac{dC_m}{dx} + \zeta'' C_m (N_{H_2O}^{M} + N_m^{M}) \tag{21}$$

Methanol balance on the anode catalyst layer (AD/M interface) is

$$N_m^{M} = N_m^{AD} - \frac{I}{6F} \tag{22}$$

Integration of Eq. (21) with the aid of Eqs. (19), (20) and (22), one obtains:

$$C_m = \frac{N_m^{AD} - I/6F}{\zeta''(N_{H_2O}^{AD} + N_m^{AD} - I/3F)} + \left\{ \frac{N_m^{AD}}{\zeta''(N_{H_2O}^{AD} + N_m^{AD})} \left[1 - \exp\left(\frac{\zeta''(N_{H_2O}^{AD} + N_m^{AD})L_{AD}}{D_m^{AD}}\right)\right] + C_m^b \exp\left(\frac{\zeta''(N_{H_2O}^{AD} + N_m^{AD})L_{AD}}{D_m^{AD}}\right) - \frac{N_m^{AD} - I/6F}{\zeta''(N_{H_2O}^{AD} + N_m^{AD} - I/3F)} \right\} \exp\left(\frac{\zeta''(N_{H_2O}^{AD} + N_m^{AD} - I/3F)(x - L_{AD})}{D_m^{M}}\right) \quad (23)$$

Due to the high cathode over-potential for methanol oxidation, methanol is consumed instantaneously at the M/CD interface [11,13], that is, $C_m(x = L_{AD} + L_M) = 0$, we have:

$$0 = \frac{N_m^{AD} - I/6F}{\zeta''(N_{H_2O}^{AD} + N_m^{AD} - I/3F)} + \left\{ \frac{N_m^{AD}}{\zeta''(N_{H_2O}^{AD} + N_m^{AD})} \left[1 - \exp\left(\frac{\zeta''(N_{H_2O}^{AD} + N_m^{AD})L_{AD}}{D_m^{AD}}\right)\right] - \frac{N_m^{AD} - I/6F}{\zeta''(N_{H_2O}^{AD} + N_m^{AD} - I/3F)} + C_m^b \exp\left(\frac{\zeta''(N_{H_2O}^{AD} + N_m^{AD})L_{AD}}{D_m^{AD}}\right) \right\} \exp\left(\frac{\zeta''(N_{H_2O}^{AD} + N_m^{AD} - I/3F)L_M}{D_m^{M}}\right) \quad (24)$$

2.3. Oxygen mass transport

Oxygen conservation within the cathode diffuser (CD):

$$\frac{dN_o^{CD}}{dx} = 0 \quad (25)$$

Oxygen flux is expressed as the effective diffusion in porous medium, expressed in the Bruggerman's relation:

$$N_o^{CD} = -D_o[\varepsilon_{CD}(1 - s_{M/CD})]^{1.5}\frac{dC_o}{dx} \quad (26)$$

Although the void space available for the gas passage is a function of local water saturation s, we adopt the smallest void fraction $\varepsilon_{CD}(1 - s_{M/CD})$ as a first approximation. Thus, the resistance to oxygen diffusion by water flooding is over-estimated in the present study.

N_o^{CD} is related to the oxygen partial current density:

$$N_o^{CD} = -\frac{I_o}{4F} \quad (27)$$

Oxygen concentration at M/CD interface is derived in combination of Eqs. (25)–(27):

$$C_o^{M/CD} = C_o^b - \frac{I_o L_{CD}}{4F D_o[\varepsilon_{CD}(1 - s_{M/CD})]^{1.5}} \quad (28)$$

2.4. Electrode kinetics expressions

The oxygen partial current density at cathode is expressed in Tafel equation:

$$I_o = I_{oo,ref}\frac{C_o^{M/CD}(1 - s_{M/CD})}{KC_{o,ref}}\exp\left(\frac{-\alpha_c F\eta_c}{RT}\right) \quad (29)$$

K is the solubility constant of oxygen between gas and aqueous phases $(1 - s_{M/CD})$ accounts for the fraction of available gas contact area. $I_{oo,ref} = i_{oo,ref}\, m_C a_C$, in which $i_{oo,ref}$ is the reference exchange current density of oxygen reduction, m_C the cathode catalyst loading, and a_C is the active surface area per unit catalyst mass. The anode methanol oxidation current density can be expressed similarly:

$$I = I_{om,ref}\frac{C_m^{AD/M}}{C_{m,ref}}\exp\left(\frac{\alpha_a F\eta_a}{RT}\right) \quad (30)$$

$I_{om,ref} = i_{om,ref}\, m_A a_A$, in which $i_{om,ref}$ is the reference exchange current density of methanol oxidation, m_A the anode catalyst loading, and a_A is the active surface area per unit mass of the anode catalyst.

2.5. Cell polarization expression

The cell voltage is calculated by subtracting the voltage losses of cathode $|\eta_c|$, anode η_a, and membrane $L_M I/\kappa_m$ from the thermodynamic cell potential $U_o - U_m$:

$$V_{cell} = U_o - U_m - |\eta_c| - \eta_a - \frac{L_M I}{\kappa_m} \quad (31)$$

2.6. Solution procedure

The cell polarization curve is calculated in a potentiostatic mode. For a given V_{cell}, variables η_c, η_a, I, $N_{H_2O}^{AD}$, $s_{M/CD}$, and N_m^{AD} are to be determined by Eqs. (29)–(31), (14), (15), and (24). Note that $C_o^{M/CD}$ and $C_m^{AD/M}$ in Eqs. (29)–(30) are given explicitly by Eqs. (19) and (28), while I_o in Eqs. (15), (28) and (29) is correlated by mass conservation over the entire MEA:

$$I_o = 6FN_m^{AD} \quad (32)$$

Newton–Raphson method [32] is used to solve the set of equations iteratively. The fixed parameters used in the model are listed in Table 1 unless otherwise specified.

3. Results and discussion

3.1. Membrane thickness effect

Fig. 2 depicts the cell polarization behavior of varied membrane thickness. Accompanied in this figure is the corresponding

Table 1
Fixed mass transport and kinetic parameters

Parameter	Expression	References
a_A	$52 \times 10^4\ cm^2\ g^{-1}$	[33]
a_C	$52 \times 10^4\ cm^2\ g^{-1}$	[11]
C_{H^+}	$\frac{\kappa_m RT(1000)}{F^2 D_{H^+}}$	[31]
$C_{m,ref}$	$0.5 \times 10^{-3}\ mol\ cm^{-3}$	[11]
$C_{o,ref}$	$0.496 \times 10^{-6}\ mol\ cm^{-3}$	Corresponding to the solubility of 1 atm O_2 at 353 K
D_o	$\frac{2.745\times10^{-4}}{P^C}\left(\frac{T}{\sqrt{T_{ca}T_{cb}}}\right)^{1.823}(P_{ca}P_{cb})^{0.333}(T_{ca}T_{cb})^{0.4167}\sqrt{\frac{1}{M_a}+\frac{1}{M_b}}$	[34]
D_{H^+}	$1 \times 10^{-4}\ cm^2\ s^{-1}$	[35]
D_m^{AD}	$0.1274 \times 10^{-4}\ cm^2\ s^{-1}$	[11], void fraction corrected diffusivity
D_m^M	$1.2 \times 10^{-6}\ A\ cm^{-2}$	[38]
$i_{om,ref}$	$0.7630 \times 10^{-7}\ A\ cm^{-2}$	[11]
$i_{oo,ref}$	$0.3189 \times 10^{-7}\ A\ cm^{-2}$	[36]
k_p^{AD}	$6.875 \times 10^{-9}\ cm^2$	[29]
k_p^{CD}	$6.875 \times 10^{-9}\ cm^2$	Chosen the same as k_p^{AD}
k_p^m	$2 \times 10^{-15}\ cm^2$	An average of Refs. [28,37]
K	$\frac{1}{R_g T}\exp\left(\frac{-666}{T}+14.1\right)$	[33]
L_{AD}	0.026 cm	[31]
L_{CD}	0.026 cm	[31]
L_M	0.0051, 0.0127, 0.023 cm for Nafion 112, 115, and 117	[31,36]
$n_d^{H_2O}$	2.5	[38]
M_a	$32\ g\ mol^{-1}$	[34]
M_b	$28\ g\ mol^{-1}$	[34]
P_{ca}	49.7 atm	[34]
P_{cb}	33.5 atm	[34]
T_{ca}	154.4 atm	[34]
T_{cb}	126.2 atm	[34]
U_{mo}	0.03 V	[13]
U_m	$U_{mo}+\frac{RT}{F}\ln\left(\frac{C_{H^+}}{(C_{m,ref}1000)^{1/6}}\right)$	[31], (reference pressure of CO_2 = 1 atm)
U_{oo}	$1.23-0.9\times10^{-3}(T-298)$	[31]
U_o	$U_{oo}+\frac{RT}{F}\ln C_{H^+}$	[31], (reference pressure of O_2 = 1 atm)
α_a	0.5	[27,28]
α_c	1	[28,33]
κ_m	$0.6842 \times 10^{-1}\ S\ cm^{-1}$	[11,31,39]
ε_{CD}	0.6	[23]
σ	$62.5\ g\ s^{-2}$	[29]
μ	$3.565 \times 10^{-3}\ g\ cm^{-1}\ s^{-1}$	[29,31]
ρ	$0.054\ mol\ cm^{-3}$	[31]
ζ''	$18\ g\ mol^{-1}$	Water molecular weight

methanol crossover rate expressed as the leaking current density. It is seen that methanol permeation is significant for the thinner membrane, which is declined gradually when the cell limiting current density is approached. Usually highest leaking current density is observed at the open circuit voltage; however, there are occasions that a maximum methanol crossover rate appears in the polarized region. We will come back to this point later when we discuss the methanol feed concentration effect. The coincidence of the vanishing in leaking current density with the arrival of cell limiting current density implies the dominance of anodic process for the prescribed parameters. There is a decline of cell voltage near OCV, covering the activation till the emerging of ohmic resistance controlled regime, when a thin membrane is used. The voltage loss of thin membrane is originated from the mixed potential effect. The higher methanol crossover rate induces an internal short-circuit on the cathode electrode; thus, the available cathode potential is partially consumed by the oxidation of crossed methanol on the cathode. As the discharge rate increases, the crossover effect is diminished while the membrane ohmic resistance dominates as more significant for the thicker membrane. For a better illustration of the relative contributions of anode, cathode, and ohmic resistance, Fig. 3 depicts the cumulative over-potentials for Nafion 112 and 117. As shown in this plot, Nafion 112 has larger cathode over-potential $|\eta_c|$ than that of 117 due to the mixed potential effect; the difference decreases at larger discharge rate. It is interesting to note that when the anodic over-potential η_a is included, that is, the portion accounted by $U_o - U_m - |\eta_c| - \eta_a$, Nafion 112 has an overall higher over-potential than Nafion 117. This is caused by the always less methanol concentration available on the anode

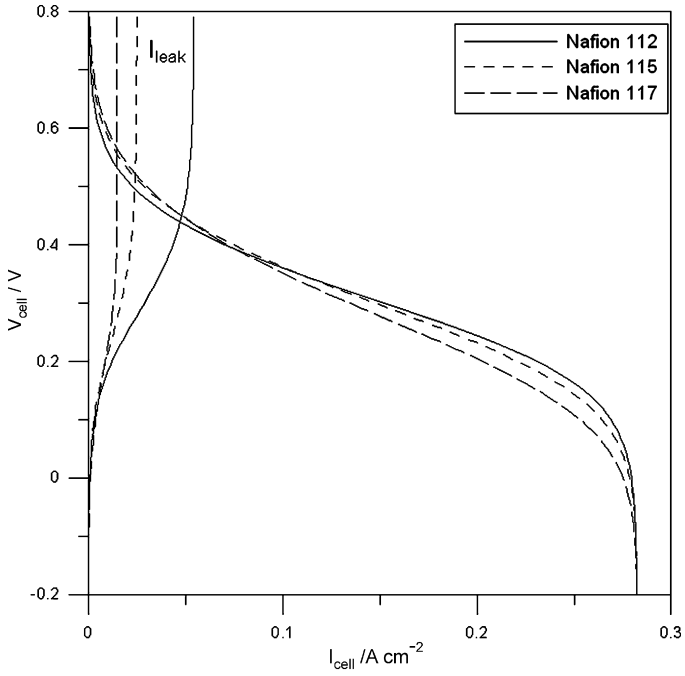

Fig. 2. Cell polarization curve with the associated leaking current density for different membrane thickness. Cathode feed: air, anode feed: methanol 0.5 M, cathode gas diffuser contact angle: 120°, $P^A = P^C = 1$ atm, $T = 353$ K.

catalyst when the thinner membrane employed. Lower concentration induces higher anode electrode over-potential η_a. This point will become clear when methanol concentration profile is shown later in Fig. 4. Finally, as the ohmic potential $L_m I_{cell}/\kappa_m$ is included, the thicker membrane has the largest polarization in the region of high discharge rates.

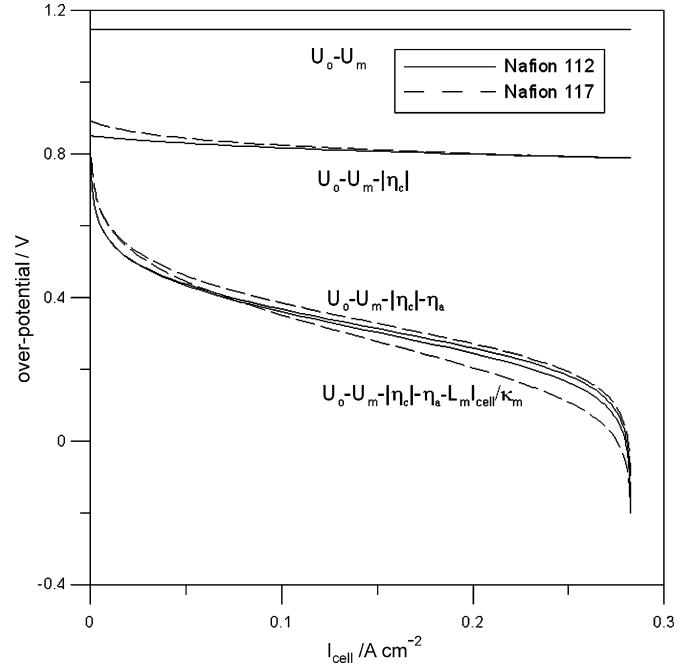

Fig. 3. Cumulative over-voltages for Nafions 112 and 117. Cathode feed: air, anode feed: methanol 0.5 M, cathode gas diffuser contact angle: 120°, $P^A = P^C = 1$ atm, $T = 353$ K.

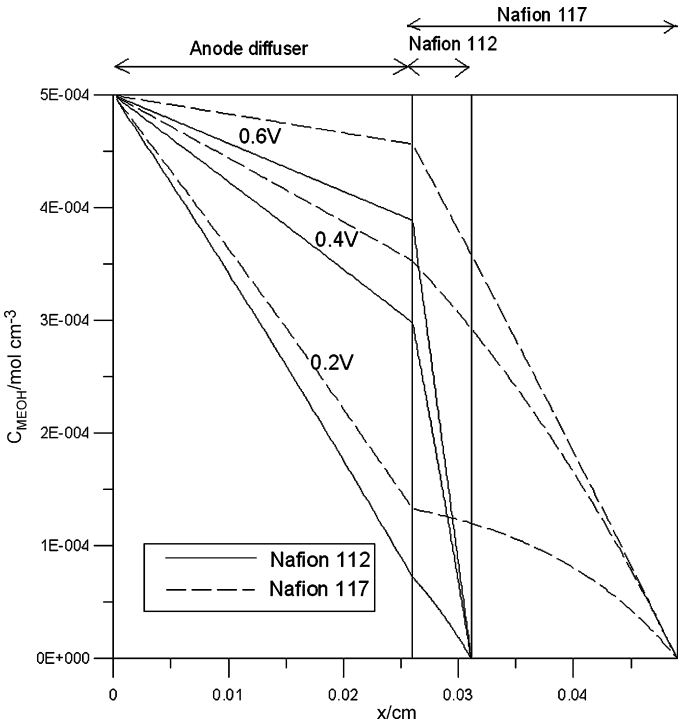

Fig. 4. Methanol concentration profiles within the anode diffuser and the membrane for Nafions 112 and 117. Cell voltages are specified at 0.6, 0.4, and 0.2 V. Cathode feed: air, anode feed: methanol 0.5 M, cathode gas diffuser contact angle: 120°, $P^A = P^C = 1$ atm, $T = 353$ K.

Detailed methanol concentration profiles are given at three cell voltages depicted in Fig. 4. It is shown at a specified potential, thicker membrane preserves a higher methanol concentration at AD/M interface. The less available concentration for thinner membrane confirms the observation of higher anode over-potential η_a in Fig. 3. It is the larger mass diffusion of methanol within thinner membrane decreases methanol concentration on the anode catalyst and, in turn increases η_a. Zhang and Wang [10] defined "the crossover over-potential" as "the difference between the cathode over-potential of a real DMFC and the ideal case with no crossover". Although the crossover phenomenon can be characterized by the rise of cathode over-potential, it is shown in the present study that crossover affects the anode potential as well, and should be noticed.

Water saturation profiles across the cathode gas diffuser in Fig. 5 are specified at the cell voltages of 0.6, 0.4 and 0.2 V. Zero saturation is presumed at the diffuser/flow channel interface in the calculation. Capillary pressure equilibrium and water transport determines the saturation profiles. As expect, a larger over-voltage induces higher water saturation caused by the significant electro-osmotic water drag through membrane and water generation at the cathode catalyst layer. Certain feature is observed in the water saturation profiles. That is, near OCV (0.6 V), thicker membrane induces higher water saturation within the cathode diffuser. This trend reverses at high over-voltage (0.2 V). Such behavior is in parallel with the cell polarization curves in Fig. 2. For a specified voltage, the current response is in close association with the water hold up in the cathode diffuser. In addition to the water generation of oxygen

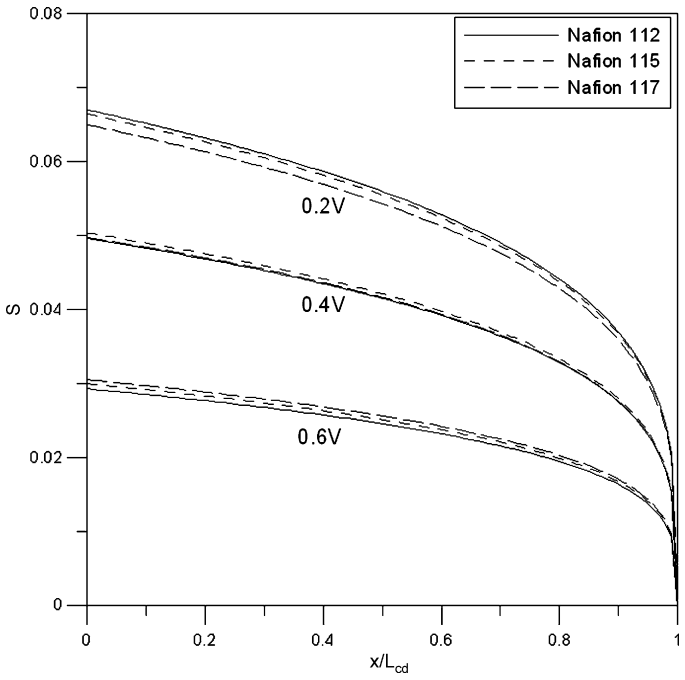

Fig. 5. Water saturation profiles within the cathode diffusion layer (CD) with varied membrane thickness. Cell voltages are specified at 0.6, 0.4, and 0.2 V. Cathode feed: air, anode feed: methanol 0.5 M, cathode gas diffuser contact angle: 120°, $P^A = P^C = 1$ atm, $T = 353$ K.

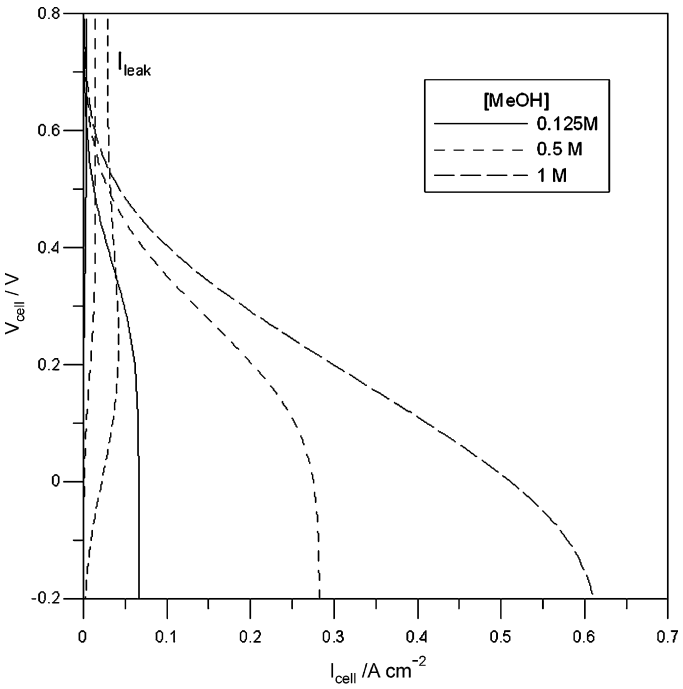

Fig. 6. Cell polarization curves with the corresponding methanol leaking current densities at various methanol feed concentrations. Cathode feed: air, membrane Nafion 117, cathode gas diffuser contact angle: 120°, $P^A = P^C = 1$ atm, $T = 353$ K.

reduction in the cathode catalyst layer, Eq. (4) indicates that the electro-osmotic drag of water in membrane is in proportion to the cell discharge rate.

3.2. Effect of methanol concentration

Fig. 6 displays the cell performance at different methanol feed concentrations. The coincidence of the approaching of cell limiting current density with the vanishing of methanol leaking current density suggests the dominance of the anodic process for the given concentrations and operating conditions. As expect, higher cell current density occurs when a high methanol concentration provided. The limiting cell current density is proportional to the methanol concentration used. However, there is peculiar feature appears when various feed concentrations are compared. There is an enhanced proportionality with methanol concentration as regard to the limiting current density. For instance, the limiting current density is over 0.6 A cm^{-2} at 1 M methanol fed, which is more than twice of that at 0.5 M. The limiting current densities when convective mass transport excluded can be calculated according to $6FD_m^{AD}(C_m^b/L_{AD})$, which give the values of 0.06514, 0.2606 and 0.5211 A cm^{-2} for methanol concentrations 0.125, 0.5 and 1 M, respectively. The model calculated limiting current densities when convective mass transport considered in Fig. 6 are 0.06639, 0.2824 and 0.6218 A cm^{-2} for the given concentrations. The enhancement is a direct consequence of the water flow-induced convective mass transfer on methanol, as described in Eqs. (17) and (21). Fig. 6 also shows that higher methanol concentration induces a higher leaking current density. Although not clear in this figure, there are interesting maximum leaking current densities appearing at 0.46 and 0.24 V for the methanol feeds of 0.5 and 1 M, respectively. Fig. 7 gives a magnified scale about the leaking current density as a function of cell current density. There is a initial rise of methanol crossover with the cell current density when the higher methanol concentration is used. The nonlinear behavior has to do with the increase of convective contribution of methanol transport as suggested in

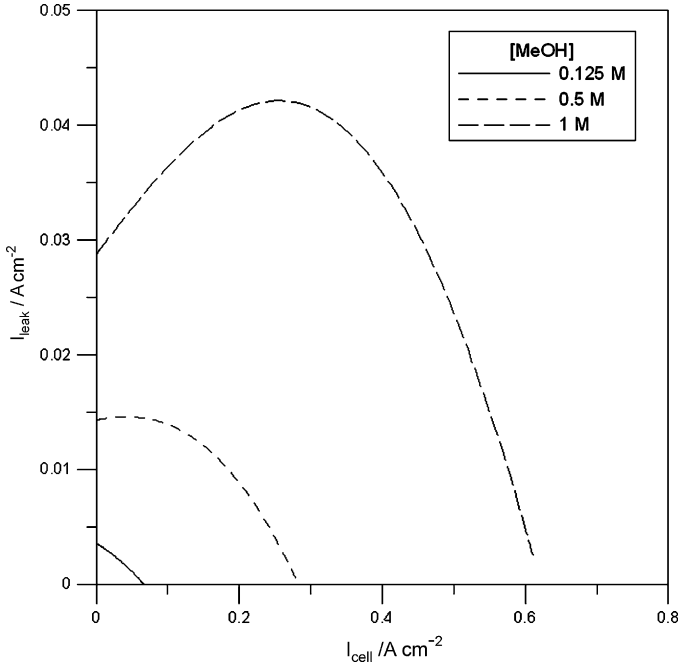

Fig. 7. Leaking current density as a function of cell current density at various methanol concentrations. Cathode feed: air, membrane Nafion 117, cathode gas diffuser contact angle: 120°, $P^A = P^C = 1$ atm, $T = 353$ K.

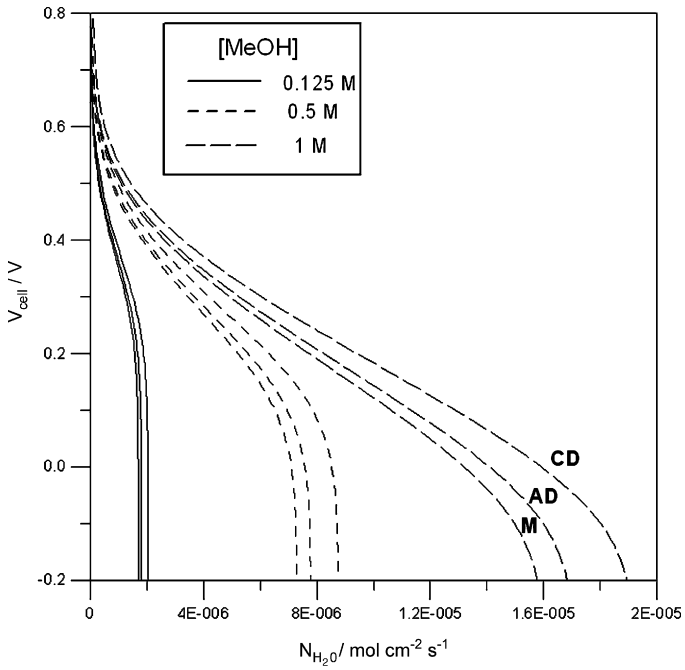

Fig. 8. Cell voltage vs. water flux rates within anode diffuser (AD), membrane (M), and cathode diffuser (CD) at various feed concentrations. Cathode feed: air, membrane Nafion 117, cathode gas diffuser contact angle: 120°, $P^A = P^C = 1$ atm, $T = 353$ K.

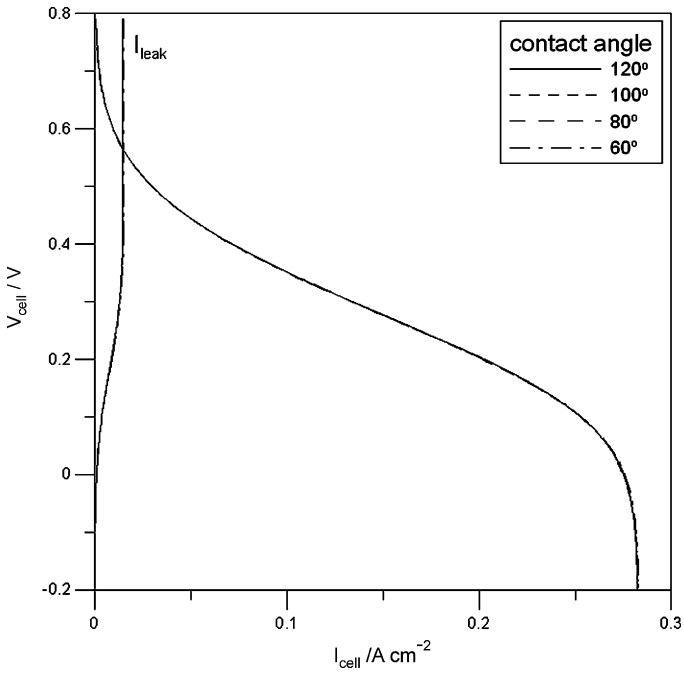

Fig. 9. Cell polarization curves with the corresponding leaking current densities at various cathode diffuser (CD) contact angles. Cathode feed: air, membrane Nafion 117, methanol 0.5 M, $P^A = P^C = 1$ atm, $T = 353$ K.

the second term on the right hand side of Eq. (21). Although the diffusive mass transfer decreases steadily with I_{cell}, there could be a situation where the enhanced methanol convection by water flow surpasses the decline of diffusion so that an overall increase of I_{leak} occurs. Eq. (4) expresses the linear increase of water flux with the cell current density. At a later stage, both mechanisms of methanol transport decrease due to the consumption of reactant at the anode catalyst. The occurring of methanol crossover maximum has to do with the anode catalyst activity, methanol feed concentration, and the transport parameters within the diffusion media. Similar observation was found by other researchers [27,28], and even in the direct ethanol fuel cell systems [40,41].

Fig. 8 illustrates the respective water fluxes through the anode diffuser (AD), membrane (M), and cathode diffuser (CD) with the cell voltages. The water discharge rate is in parallel with the polarization curve. Eqs. (2), (9) and (10) determine the distribution of water fluxes within various media of the MEA. Though not shown here, higher methanol concentration also induces higher water saturation in cathode diffuser and higher back-pressure through the membrane.

3.3. Inference of contact angle in the cathode diffuser

In addition to the permeability and porosity of the gas diffusion layer, the water transport depends on the hydrophobicity of the layer, which is normally characterized by the contact angle between liquid water and carbon fiber matrix as shown in Eq. (7). Lim and Wang [18] in the study of proton exchange fuel cells showed that for various contents of fluorinated ethylene propylene (FEP) added in the layer, the contact angles measured were decreased rapidly with temperature showing a transition from hydrophobic ($\theta_c > 90°$) to hydrophilic property ($\theta_c < 90°$). That is, hydrophobic property of the diffuser may change with the operating conditions. Fig. 9 depicts the simulated polarization curves for a range of contact angles in the CD. The corresponding leaking current densities are included as well. There is hardly any significant variation of cell current density with the contact angle under the specified MEA structure and mass transport parameters. The reason for that is the predicted saturation within the CD is low (always less than 10%) so that there is only minor pore blocking effect on gaseous oxygen transport in the CD. In addition, the cell discharge is mainly limited by the anodic reaction so that characteristics in the cathode diffuser have insignificant influence on the MEA performance.

Liquid pressure at M/CD interface $P^{M/CD}$ along with the cell voltage at different CD contact angles is demonstrated in Fig. 10. Liquid pressure at AD/M interface is also included, which is nearly constant during the discharge process. That is, the second term on the right side of Eq. (12) is negligible. $P^{M/CD}$ at OCV depends on the water generation at mixed potential of the cathode and the associated capillary pressure equilibrium on the water saturation. Positive capillary pressure is developed for the hydrophobic medium, while negative capillary pressure is for the hydrophilic diffuser. It seems the magnitude of the capillary pressure, $|P_c|$, for the hydrophilic medium is much larger than that of hydrophobic medium. In addition, the liquid pressure $P^{M/CD}$ always increases with the cell voltage, as the result of increased water saturation, indifferent to the hydrophobicity of the CD. Thus, a positive increase of $(P^{M/CD} - P^{AD/M})/L_m$ with over-voltage is developed for the hydrophobic diffuser, and an increased back-pressure is induced as indicated in the first term on the right side of Eq. (4). The corresponding water fluxes in different domains of the MEA are demonstrated in Fig. 11. It is

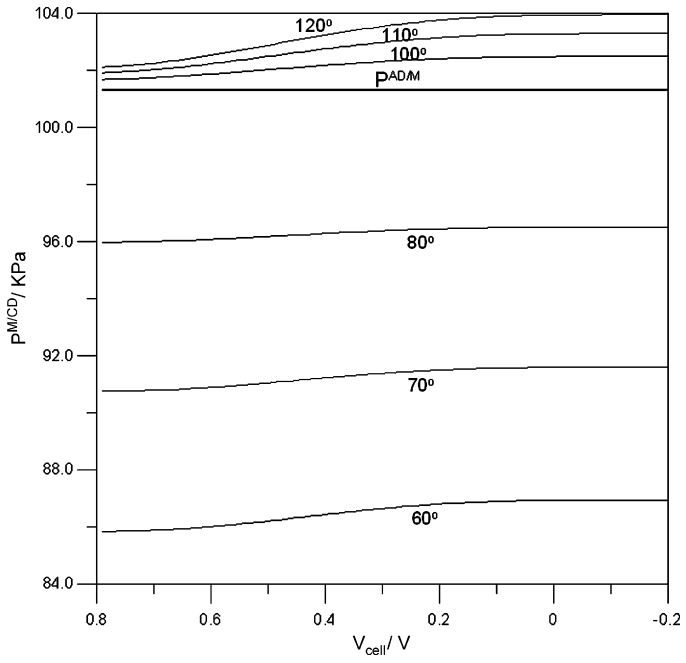

Fig. 10. Liquid pressure at membrane/cathode diffuser interface vs. cell voltage at various cathode diffuser contact angles. Cathode feed: air, membrane Nafion 117, methanol 0.5 M, $P^A = P^C = 1$ atm, $T = 353$ K.

clear that higher water flux occurs in each domain when the CD becomes more hydrophilic. As discussed earlier, water flooding in the CD is not severe so that no significant impact on the polarization curve is observed in Fig. 9. However, it should be mentioned that there is minor difference in Fig. 9 at high discharge rate if magnified scale is plotted, due to the increased

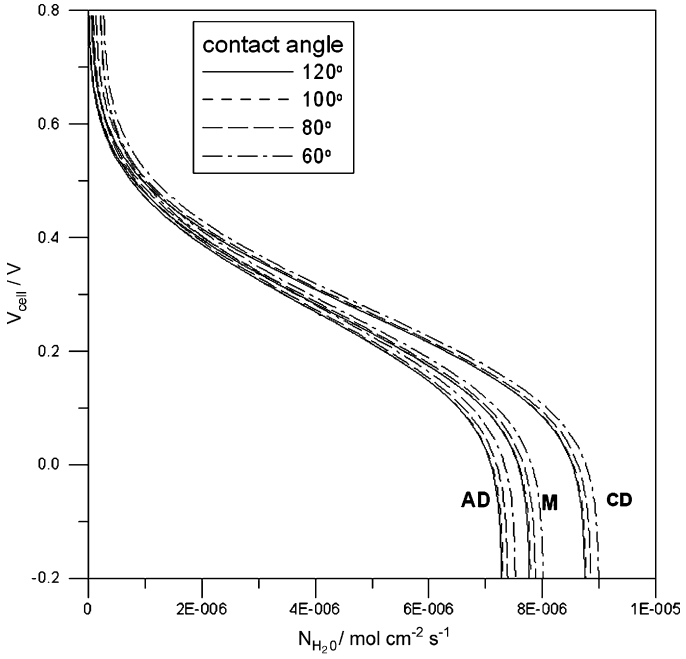

Fig. 11. Cell voltage vs. water flux rates within anode diffuser (AD), membrane (M), and cathode diffuser (CD) at various cathode diffuser contact angles. Cathode feed: air, membrane Nafion 117, methanol 0.5 M, $P^A = P^C = 1$ atm, $T = 353$ K.

back-pressure within the membrane as justified in Fig. 10 and Eq. (4). Fig. 11 indicates that the hydrophobic layer indeed has a better capability in inhibiting the water flow. To extend the back-pressure for preventing water flux, an extra thin hydrophobic micro-layer may be added to the M/CD interface as did by Xu et al. [20] and Pasaogullari et al. [37].

4. Conclusion

Analytical mass transfer equations on the membrane electrode assembly of direct methanol fuel cell are formulated, which give explicitly the inter-relationship of methanol crossover and water transport rate. The cell voltage drop caused by the methanol crossover is evaluated by the mixed potential theory on the parasitic oxygen reduction and methanol oxidation occurring on the cathode catalyst. Water flux rate, methanol concentration, oxygen gas concentration, liquid pressure distribution and water saturation in the MEA can be simulated in corporation with the given electrochemical kinetics.

According to the model prediction, larger voltage drop occurs near OCV due to the mixed potential effect when the thinner membrane is used; however, the voltage gained at larger polarization benefits from the smaller ohmic resistance as compared to the thicker membrane. It is also pointed out the methanol crossover not only affects the cathode over-potential but also varies the methanol concentration distribution near the anode, and alters the anode over-potential. In the study of methanol feed concentration effect, it is shown that the convective contribution on methanol crossover by water flux may surpass the decrease of diffusion mechanism in the early stage of cell discharge, causing a maximum on the leaking current density. Hydrophobic treatment on the cathode diffusion layer seems not affect the polarization behavior when the CD water saturation is not high enough to block the gas passage. However, the water flux predicted is indeed a function of surface contact angle, and less water flux is observed when using the hydrophobic layer because of the induced back-pressure across the membrane.

Acknowledgements

The author is indebted to Lili Cheng for her assistance in so many aspects in the preparation of this manuscript. The author is grateful for the financial support from National Science Council of the Republic of China (NSC 96-2221-E-155-049), without which the research on fuel cells could never be possible. Fig. 1 is prepared by C.-Y. Yang.

Appendix A. Nomenclature

a_A	active area per unit mass of anode catalyst ($cm^2\ g^{-1}$)
a_C	active area per unit mass of cathode catalyst ($cm^2\ g^{-1}$)
C_{H^+}	proton concentration in membrane phase ($mol\ dm^{-3}$)
C_m	methanol concentration ($mol\ cm^{-3}$)
$C_{m,ref}$	reference methanol concentration ($mol\ cm^{-3}$)
C_o	oxygen concentration ($mol\ cm^{-3}$)
$C_{o,ref}$	reference oxygen concentration ($mol\ cm^{-3}$)

C_m^b methanol concentration in the anode flow channel ($mol\,cm^{-3}$)
$C_m^{AD/M}$ methanol concentration at anode diffuser/membrane interface ($mol\,cm^{-3}$)
C_o^b oxygen gas concentration in the cathode flow channel ($mol\,cm^{-3}$)
$C_o^{M/CD}$ oxygen gas concentration at membrane/cathode diffuser interface ($mol\,cm^{-3}$)
D_{H^+} proton diffusivity in membrane ($cm^2\,s^{-1}$)
D_o oxygen gas diffusivity in cathode gas diffuser ($cm^2\,s^{-1}$)
D_m^{AD} methanol diffusivity in the anode diffuser ($cm^2\,s^{-1}$)
D_m^M methanol diffusivity in the membrane ($cm^2\,s^{-1}$)
F Faraday constant ($96{,}500\,C\,mol^{-1}$)
$i_{om,ref}$ reference methanol oxidation exchange current density ($A\,cm^{-2}$)
$i_{oo,ref}$ reference oxygen reduction exchange current density ($A\,cm^{-2}$)
I cell current density ($A\,cm^{-2}$)
I_{leak} crossover current density ($A\,cm^{-2}$)
I_o oxygen reduction current density ($A\,cm^{-2}$)
$I_{om,ref}$ $i_{om,ref}\,m_A a_A$ ($A\,cm^{-2}$)
$I_{oo,ref}$ $i_{oo,ref}\,m_c a_c$ ($A\,cm^{-2}$)
k_p^{AD} anode diffuser liquid permeability (cm^2)
k_p^{CD} cathode diffuser liquid permeability (cm^2)
k_p^M membrane liquid permeability (cm^2)
k_{rl}^{CD} liquid phase relative permeability in cathode diffuser
K solubility constant of oxygen in liquid phase
L_{AD} anode backing layer thickness (cm)
L_{CD} cathode gas diffuser thickness (cm)
L_M membrane thickness (cm)
m_A anode catalyst loading ($g\,cm^{-2}$)
m_C cathode catalyst loading ($g\,cm^{-2}$)
M_a molecular weight of O_2 ($g\,cm^{-2}$)
M_b molecular weight of N_2 ($g\,cm^{-2}$)
$n_d^{H_2O}$ electro-osmotic drag coefficient
$N_{H_2O}^{AD}$ water flux in anode diffuser ($mol\,cm^{-2}\,s^{-1}$)
$N_{H_2O}^{CD}$ water flux in cathode diffuser ($mol\,cm^{-2}\,s^{-1}$)
$N_{H_2O}^{M}$ water flux in membrane ($mol\,cm^{-2}\,s^{-1}$)
N_m^{AD} methanol flux in anode diffuser ($mol\,cm^{-2}\,s^{-1}$)
N_m^M methanol flux in membrane ($mol\,cm^{-2}\,s^{-1}$)
N_o^{CD} oxygen gas flux in cathode diffuser ($mol\,cm^{-2}\,s^{-1}$)
P_c capillary pressure ($g\,cm^{-1}\,s^{-2}$)
P_{ca} critical pressure of O_2 (atm)
P_{cb} critical pressure of N_2 (atm)
P_l liquid pressure ($g\,cm^{-1}\,s^{-2}$)
P^A anode pressure ($g\,cm^{-1}\,s^{-2}$)
$P^{AD/M}$ liquid pressure at anode diffuser/membrane ($g\,cm^{-1}\,s^{-2}$)
P^C cathode pressure ($g\,cm^{-1}\,s^{-2}$)
$P^{M/CD}$ liquid pressure at membrane/cathode diffuser ($g\,cm^{-1}\,s^{-2}$)
R universal gas constant ($8.314\,J\,mol^{-1}\,K^{-1}$)
R_g universal gas constant ($82.06\,atm\,cm^3\,mol^{-1}\,K^{-1}$)
s water saturation in cathode diffuser
$s_{M/CD}$ water saturation at membrane/cathode diffuser interface
T absolute temperature (K)
T_{ca} critical temperature of O_2 (K)
T_{cb} critical temperature of N_2 (K)
U_m reference methanol oxidation open circuit potential (V)
U_{mo} standard potential of methanol oxidation (V)
U_o reference oxygen reduction open circuit potential (V)
U_{oo} standard potential of oxygen reduction (V)
V_{cell} cell voltage (V)

Greek letters

α_a anodic transfer coefficient of methanol oxidation
α_c cathodic transfer coefficient of oxygen reduction
ε_{CD} void fraction in cathode gas diffuser
ζ'' molecular weight of water ($g\,mol^{-1}$)
η_a electrode over-potential in anode (V)
η_c electrode over-potential in cathode (V)
θ_c contact angle (rad)
κ_m proton conductivity in membrane phase ($S\,cm^{-1}$)
μ viscosity of water ($g\,cm^{-1}\,s^{-1}$)
ν kinematic viscosity ($g\,cm^2\,s^{-1}\,mol^{-1}$)
ρ liquid water molar density ($mol\,cm^{-3}$)
σ surface tension ($g\,s^{-2}$)

References

[1] H. Dohle, K. Wippermann, J. Power Sources 135 (2004) 152.
[2] M. Baldauf, W. Preidel, J. Power Sources 84 (1999) 161.
[3] S. Hikita, K. Yamane, Y. Nakajima, JSAE Rev. 22 (2001) 151.
[4] R. Jiang, D. Chu, J. Electrochem. Soc. 151 (1) (2004) A69.
[5] C.-H. Chen, T.-K. Yeh, J. Power Sources 160 (2006) 1131.
[6] J. Cruickshank, K. Scott, J. Power Sources 70 (1998) 40.
[7] K. Scott, P. Argyropoulos, K. Sundmacher, J. Electroanal. Chem. 477 (1999) 97.
[8] A.A. Kulikovsky, Electrochem. Commun. 6 (2004) 1259.
[9] A.A. Kulikovsky, J. Electrochem. Soc. 152 (6) (2005) A1121.
[10] J. Zhang, Y. Wang, Fuel Cells 4 (2004) 90.
[11] K.-M. Yin, J. Power Sources 167 (2007) 420.
[12] F. Liu, C.-Y. Wang, J. Electrochem. Soc. 154 (6) (2007) 514.
[13] B.L. Garcia, V.A. Sethuraman, J.W. Weidner, R.E. White, R. Dougal, J. Fuel Cell Sci. Technol. 1 (2004) 43.
[14] A. Blum, T. Duvdevani, M. Philosoph, N. Rudoy, E. Peled, J. Power Sources 117 (2003) 22.
[15] E. Peled, A. Blum, A. Aharon, M. Philosoph, Y. Lavi, Electrochem. Solid-State Lett. 6 (12) (2003) A268.
[16] G.Q. Lu, F.Q. Liu, C.-Y. Wang, Electrochem. Solid-State Lett. 8 (1) (2005) A1.
[17] F. Liu, G. Lu, C.Y. Wang, J. Electrochem. Soc. 153 (3) (2006) A543.
[18] C. Lim, C.Y. Wang, Electrochim. Acta 49 (2004) 4149.
[19] C. Xu, T.S. Zhao, J. Power Sources 168 (2007) 143.
[20] C. Xu, T.S. Zhao, Y.L. He, J. Power Sources 171 (2007) 268.
[21] S.S. Sandhu, R.O. Crowther, J.P. Fellner, Electrochim. Acta 50 (2005) 3985.
[22] M.H. Shi, J. Wang, Y.P. Chen, J. Power Sources 166 (2007) 303.
[23] J. Rice, A. Faghri, Int. J. Heat Mass Trans. 49 (2006) 4804.
[24] W. Liu, C.-Y. Wang, J. Electrochem. Soc. 154 (3) (2007) B352.
[25] W. Liu, C.-Y. Wang, J. Power Sources 164 (2007) 561.
[26] W. Liu, C.-Y. Wang, J. Power Sources 164 (2007) 189.
[27] W.W. Yang, T.S. Zhao, Electrochim. Acta 52 (2007) 6125.
[28] J. Ge, H. Liu, J. Power Sources 163 (2007) 907.
[29] U. Pasaogullari, C.Y. Wang, J. Electrochem. Soc. 151 (3) (2004) A399.
[30] C.Y. Wang, P. Cheng, Adv. Heat Trans. 30 (1997) 93.
[31] D.M. Bernardi, M.W. Verbrugge, AIChE J. 37 (1991) 1151.

[32] B.A. Finlayson, Nonlinear Analysis in Chemical Engineering, McGraw-Hill, 1980.
[33] C. Marr, X. Li, J. Power Sources 77 (1999) 17.
[34] R.B. Bird, W.E. Stewart, E.N. Lightfoot, Transport Phenomena, Wiley, New York, 1960.
[35] J.S. Newman, Electrochemical Systems, second ed., Prentice-Hall, 1991.
[36] K.-M. Yin, J. Electrochem. Soc. 152 (3) (2005) A583.
[37] U. Pasaogullari, C.Y. Wang, K.S. Chen, J. Electrochem. Soc. 152 (8) (2005) A1574.
[38] X.M. Ren, T.E. Springer, T.A. Zawodzinski, S. Gottesfeld, J. Electrochem. Soc. 147 (2) (2000) 466.
[39] Q. Wang, M. Eikerling, D. Song, Z.-S. Liu, J. Electrochem. Soc. 154 (6) (2007) F95.
[40] G. Andreadis, S. Song, P. Tsiakaras, J. Power Sources 157 (2006) 657.
[41] G. Andreadis, P. Tsiakaras, Chem. Eng. Sci. 61 (2006) 7497.